Journal of Power Sources 221 (2013) 290–299

Contents lists available at SciVerse ScienceDirect

Journal of Power Sources

journal homepage: www.elsevier.com/locate/jpowsour

Time independent and time dependent probability of failure of solid oxide fuel cells by stress analysis and the Weibull method

R. Clague*, A.J. Marquis, N.P. Brandon

Imperial College London, South Kensington Campus, London SW7 2AZ, United Kingdom

HIGHLIGHTS

- Instantaneous and time dependent probability of failure of an SOFC has been determined over a life cycle.
- For this, anode supported, cell the cathode layer has the highest instantaneous probability of failure.
- Failure probability of all layers increases significantly over time due to slow crack growth.
- The POF was 20 times larger for an operational temperature distribution compared to a uniform 800 °C.
- A cumulative density function is defined to account for a 'lifetime' probability of failure.

ARTICLE INFO

Article history:
Received 7 May 2012
Received in revised form
15 July 2012
Accepted 31 July 2012
Available online 9 August 2012

Keywords:
SOFC
Probability
Failure
Weibull
Time
Dependent

ABSTRACT

A prediction of the probability of failure of the ceramic layers of a Solid Oxide Fuel Cell (SOFC) has been made by combining the weakest link theory and the Weibull method. Analytical and finite element models of a single, anode supported solid oxide fuel cell were developed in order to predict the stress levels in the ceramic components of an SOFC subjected to an idealised operating duty cycle representing cooling from sintering, warming to a uniform temperature of 800 °C where anode chemical reduction takes place, operation at low, medium and high power and finally cooling to room temperature. The results of this analysis are the basis of an analysis of the time independent probability of failure of the ceramic components using both an analytical approach and the CARES™ software. CARES was also used to determine *time dependent* probability of failure, which takes into account the degradation of ceramic bulk failure strength over time by the slow growth of inherent flaws. The results indicate that the probability of failure of the individual layer volumes of a solid oxide fuel cell increases significantly over time due to slow crack growth.

1. Introduction

Ceramics like those used in Solid Oxide Fuel Cells are brittle materials and as such their bulk failure strength is dependent on the number and size of inherent flaws from manufacturing that act as stress concentrations. Ceramics typically exhibit a large spread of bulk failure strength due to the random nature of these flaws. As the failure stress of brittle materials is not a well defined number a probabilistic metric is normally derived to assess whether the material will fail or not, known as the probability of failure at a given stress. Under certain conditions these flaws can enlarge over time, which has the effect of reducing the effective bulk failure strength as time goes on. When the growth of flaws is *not* considered the probability of failure is said to be 'time independent', when the growth of flaws over time is taken into account the probability of failure is said to be 'time dependent'.

The CARES (Ceramic Analysis and Reliability Evaluation of Structures) computer code is used here to predict both the time independent and time dependent probability of failure of a solid oxide fuel cell membrane subjected to an idealised operating cycle consisting of cooling from manufacture (sintering), warming to operating temperature, chemical reduction of the NiO anode, operating at three different current densities and finally cooling to room temperature. The relevant material properties for this type of analysis have been taken from the literature. Also presented within this paper is an analytical calculation of the time-independent probability of failure in each layer of a SOFC ceramic membrane subjected to uniform heating using the weakest link theory and the Weibull distribution of material failure strengths. It should be noted

* Corresponding author.
E-mail addresses: r.clague@imperial.ac.uk, ralph.clague@gordonmurraydesign.com (R. Clague).

0378-7753/$ – see front matter © 2012 Elsevier B.V. All rights reserved.
http://dx.doi.org/10.1016/j.jpowsour.2012.07.116

that the probability of failure calculations presented in this paper are for the ceramic volumes only, no attempt has been made to assess the probability of delamination, but this seems a logical next step for the work given the nature of observed SOFC failures.

2. Literature review

The first experiments indicating that the failure strengths of some materials are volume dependent and therefore dependent on the *probability* of a critical flaw being present, were performed by Leonardo Da Vinci using thin cast iron rods loaded in tension [15]. As the rods broke the pieces were again loaded to failure, the results showed an increasing failure strength with decreasing rod length. This 'volume effect' is a characteristic of brittle materials. Pierce [29] and Weibull [27] independently devised mathematical distributions to fit the spread of brittle material failure strength data. Pierce assumed the failure strengths would follow a Gaussian distribution whereas Weibull applied a more flexible distribution originally formulated by Rosin et al. [23] to describe the distribution of particle sizes in crushed coal. This is now commonly called the 'Weibull distribution' despite it's origins. Since then researchers such as Shih [25] have shown that the Weibull distribution is a more accurate representation of ceramic failure strength scatter than several other distributions including the Gaussian distribution. The Weibull distribution has many applications and forms [21] but in this paper only the two and three-parameter models are considered. The two models are basically the same except that in the latter case the third parameter is a 'threshold' stress below which no failure can occur. If this is taken as zero the model reduces to the two-parameter version.

Masson et al. [16] have studied the validity of the two or three parameter models using Monte-Carlo simulations and concluded that the decision to use a two-parameter or three-parameter model should be based on sound physical reasoning i.e. is there any reason why a threshold stress would be present? For example, a compressive surface stress generated from rapid skin cooling of the structure, or proof tested components that have a defined minimum strength.

Material data for time-independent failure of SOFC materials, commonly called the 'Weibull parameters', have been measured by researchers such as Atkinson et al. [2], Lowrie et al. [14] and Sammes et al. [28]. Selimovic et al. [24] approached the failure strength scatter problem by comparing the predicted stresses in ceramic layers to the allowable stress calculated by Montross et al. [17] for a probability of failure of 1×10^{-5} and 1×10^{-6}. Whether the layers had the same volume as those in Selimovic's model is not stated and is important as the probability of failure at a given stress is material volume dependent. Nakajo et al. [18] explored the evolution of the probability of fast fracture of a cathode supported tubular SOFC over warm up and cool down cycles using an axisymmetric model assuming a uniform temperature during warming or cooling, with temperature gradients generated from a 1D model during the electricity production phase of the cycle. Their results indicate a high probability of failure at room temperature, which decreases as the cell is warmed and then increases again as the cell produces electricity.

A large amount of work on brittle material failure modelling has been done at the NASA Glenn Research Centre in developing a comprehensive brittle material design computer program, CARES. Initially the program was developed (under the name SCARE) by Gyekenyesi [13] as a postprocessor for the MSC/Nastran finite element code, to calculate the elemental probabilities of failure based on a maximum principal stress criteria, then taking the product of these probabilities to determine the overall probability of failure of a structure [19]. Since then it has been extended several times to account for stress multi-axiality, different flaw shapes and locations and time dependent failure modes such as slow crack growth [19]. An overview of the steps in a CARES analysis are shown in Fig. 1. No evidence has been found in the literature of the application of the CARES code to the failure of ceramic components of an SOFC.

Delayed failure of brittle materials such as 8YSZ due to subcritical crack growth (SCG) over time is a well documented phenomena with researchers such as Lowrie et al. [14], Radovic et al. [22] and Choi et al. [7,6] all observing SCG effects in YSZ and LSM at room temperature and SOFC operating temperatures. The CARES computer code is able to accommodate SCG by assuming that flaws grow in size as a function of stress and temperature according to a power law, thus lowering the critical stress intensity required to produce fracture over time. Time dependent failure mechanisms have not been included in any coupled SOFC analyses to date.

2.1. Time independent probability of failure

The time-independent failure probability of a structure is the probability of fast fracture of a structure in the instant after a load is applied without taking into account any load history or historical material degradation. The weakest link theory can be used to calculate the probability of failure of a structure subjected to a uniform uniaxial load by considering it to be analogous to a chain in tension with n links, each with a different failure strength. When the weakest link fails, the whole structure will fail and therefore the bulk strength of the chain is dependent on the weakest link. If the distribution of failure strengths is known then for a given load the probability that a single link will fail can be calculated [27]. The probability of any one of the n links having a limiting strength below the applied load is then the product of the individual failure probabilities. Weibull [27] expressed the probability of failure of the i-th link $P_{f,i}$, with a volume V_i, subjected to a uniform uniaxial stress σ, in integral form as

$$P_{f,i} = 1 - \exp\left[- \int_{V_i} \left(\frac{\sigma - \sigma_{th}}{\sigma_0} \right)^m dV_i \right] \quad (1)$$

where σ_{th} is the threshold stress below which no failures can occur, m is the Weibull modulus and the 'scale parameter' σ_0, is a material property defined as the stress at which the probability of failure of a unit volume of material is 0.632. This is referred to as Weibull's three parameter model. For a given applied stress, the probability of failure of the structure is then

$$P_{f,structure} = 1 - \prod_{i=1}^{n} \left(1 - P_{f,i} \right) \quad (2)$$

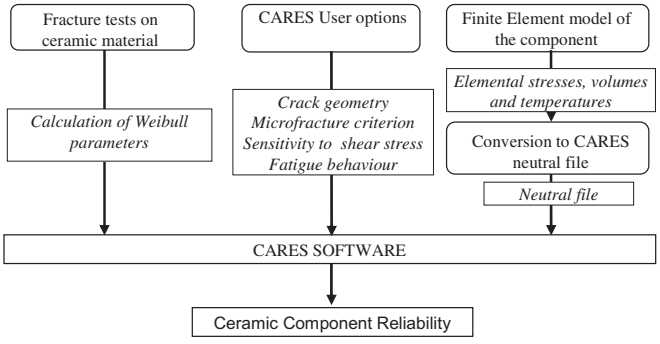

Fig. 1. CARES analysis overview [19].

It is common for σ_{th} to be taken as zero in which case the probability of failure equation reduces to the two parameter form

$$P_f = 1 - \exp\left[- \int_V \left(\frac{\sigma}{\sigma_0}\right)^m dV \right] \quad (3)$$

From Equations (1) and (3) it can be seen that P_f is directly dependent on specimen volume, with the probability of failure increasing with increasing volume for a given applied stress. This is known as the 'volume effect' and is physically consistent with a larger volume containing a physically larger flaw which in turn generates a larger stress intensity K, for a given far field tensile stress as shown in Fig. 2.

The Weibull scale parameter σ_0, is a material property associated with a unit volume of material. To measure it directly a statistically significant number of samples of unit volume would have to be tested to failure. To calculate σ_0 from component tests that are not unit volume the characteristic strength σ_θ, of a structure is defined as the uniform, uniaxial stress at which the probability of failure of that structure is 0.632. Considering the applied stress to be σ_0 a relationship between the characteristic strength σ_θ, and the scale parameter σ_0, can then be defined as in Equation (4)

$$0.632 = 1 - \exp\left[- \left(\frac{\sigma_\theta}{\sigma_0}\right)^m V_e \right] \quad (4)$$

such that an 'effective volume' relating the characteristic strength, which is a property of an individual structure, to the scale parameter, which is a material property, is given by Equation (5).

$$V_e = \left(\frac{\sigma_0}{\sigma_\theta}\right)^m \quad (5)$$

The calculation of the scale parameter, σ_0 is often omitted from studies of ceramic failure strength distribution in the literature, normally only the characteristic strength is presented. This makes it difficult to use data in the literature for the analysis of geometries and loading situations different to the test piece geometry and test loads without re-analysing the data to calculate the scale parameter from (5), which is covered more thoroughly in Section 2.2.

When the load is time varying a cumulative distribution function (CDF) is defined as the maximum probability of failure experienced by a component over the time period of interest.

So far the discussion of the weakest link theory and Weibull strength distribution in this paper have assumed uniform, uniaxial stress distributions. In many operational loading situations the stress field in a component is multi-axial. A number of methods exist to account for multi-axiality such as; the Principle of Independent Action (PIA) [19]; Normal Stress Averaging (NSA) [12,19]; or using a mechanistic model taking into account crack orientation as well as stress multi-axiality [26,5].

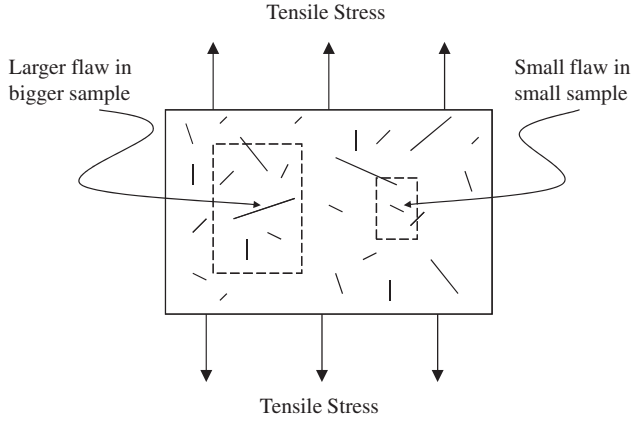

Fig. 2. Volume dependence on sample strength resulting from distribution of flaw sizes [1].

2.2. Time independent material properties

The material properties necessary for the probability of failure calculation are the Weibull modulus m, the Weibull scale parameter σ_0, and the threshold stress σ_{th}. Linearising Equation (3) by taking the logarithm of both sides twice yields (6), the equation of a straight line with slope equal to m, and intercept of $\ln(1/\sigma_\theta)^m$

$$\ln\left[\ln\left(\frac{1}{1-P_f}\right)\right] = m\ln(\sigma) + \ln\left(\frac{1}{\sigma_\theta}\right)^m \quad (6)$$

When $\ln\ln(1/(1-P_f))$ is plotted against $\ln(\sigma)$ for the experimental data it is then possible to fit a straight line through the points from the equation of the line calculate m and σ_θ. In order to calculate the material property, σ_0 from the characteristic strength of the structure, σ_θ using Equation (5) it is necessary to determine the effective volume, V_e. For a four point bend test V_e is defined [20] as

$$V_e = \frac{wh}{2}\frac{(L_1 + mL_2)}{(m+1)^2} \quad (7)$$

where w is the width of the beam, h is the beam height, L_1 and L_2 are the distances between the supports and loads respectively. Each different loading configuration has a unique expression for V_e and this must be taken into account when calculating the Weibull parameters from material tests other than pure tensile tests.

Atkinson et al. [4] determined the Weibull modulus and Weibull characteristic strength for some common ceramics used in SOFCs using a ring-on-ring testing configuration. The test specimen was a circular disc of diameter 23 mm and 200 μm thickness giving a specimen volume of 8.31×10^{-8} m^3, which has then taken to be equal to the effective volume V_e for the calculation of the Weibull scale parameter using Equation (5). These material properties are summarised in Table 1.

The error in the calculation of characteristic strength and scale parameter using Equation (6) could be perceived as quite large, as it is calculated from a best fit line on a loglog vs log plot. In the original paper by Selcuk the error on the characteristic strength was given as ±15%, no error bars were given for the Weibull modulus. For both YSZ (and Ni/YSZ) the values of characteristic strength decrease with temperature, indicating that the material is on average, weaker at higher temperatures. The Weibull modulus m, of YSZ (and Ni/YSZ) increases with increasing temperature, indicating that the spread of failure strengths (not necessarily the magnitude of the failure strengths) of the specimens tested has become narrower at higher temperatures. This is behaviour typical of more ductile materials and makes physical sense when the mechanisms of ductility (plasticity at crack tips) are considered: at higher

Table 1
Weibull parameters of SOFC materials.

	σ_θ(MPa)		m		σ_0(MPa)	
	25 °C	800 °C	25 °C	800 °C	25 °C	800 °C
YSZ	232 [4]	154 [4]	5.7 [4]	8.6 [4]	13.3	23.1
LSM	52 [4]	75 [4]	6.7 [4]	3.7 [4]	4.56	0.915
NiO–YSZ	187 [4]	124[a]	11.8 [4]	17.8[a]	47	49.6

[a] Calculated here assuming same temperature dependence as pure YSZ.

temperatures materials are typically more ductile and therefore stresses at crack tips are relieved locally rather than causing to catastrophic failure of the structure.

2.3. Time dependent probability of failure

In some brittle materials there is a decrease in the bulk failure strength of a material over time due to sub-critical crack growth (SCG) as pre-existing flaws in the material bulk extend over time under non-critical stresses. Given enough time a critical flaw size a_c is reached and catastrophic failure occurs. This happens when the mode 1 stress intensity, K_1 reaches the critical value K_{1C}. It is distinct from time independent failure (which can increase or decrease over time according to the instantaneous loading), which assumes bulk material properties that are constant over time. On a plot of the logarithm of crack velocity da/dt against the logarithm of the mode 1 stress intensity factor K_1 as shown in Fig. 3, SCG can be broken down into three regimes.

In region I below a certain threshold stress intensity no SCG occurs, in region II the crack growth rate is proportional to the stress intensity and in region III the crack growth rate increases rapidly with increasing stress intensity until a critical value is reached and the crack propagation rate becomes so rapid that it is considered to be 'fast-fracture'. The lifetime of materials that exhibit SCG is dominated by region II. The rate of sub-critical crack growth in region II has been shown for brittle materials [4,6,7] to follow a power law such that the crack growth can be written as a function of the mode 1 stress intensity as presented in Equation (8).

$$\frac{da}{dt} = AK_1^{N_{scg}} \tag{8}$$

where the SCG stress exponent N_{scg} and A are constants for a given material, loading and environment. If the time to failure t_{ref} is known for a reference stress σ_{ref}, the time to failure t_f for another constant applied stress σ can be calculated according to Equation (9).

$$\frac{t_f}{t_{ref}} = \left(\frac{\sigma_{ref}}{\sigma}\right)^{N_{scg}} \tag{9}$$

2.4. Time dependent material properties

The slow crack growth exponent N_{scg}, in Equation (9) can be derived from either static or dynamic material testing. In the static case a constant stress is applied to a test specimen and the time to failure recorded. On a plot of log t_f against log σ, N_{scg} can then be obtained from the gradient of a line through the data points in accordance with the linearised form of Equation (8). In the dynamic case a statistically significant number of samples are subjected to a constant stress rate $\dot{\sigma}$, and the failure stress σ_f and time to failure are recorded. On a plot of log σ_f against log$\dot{\sigma}$ a line through the characteristic strengths at each stress rate will have gradient $1/(1+N_{scg})$ and intercept log D_{scg} according to (10), reproduced here from the testing standard ASTM C 1465.

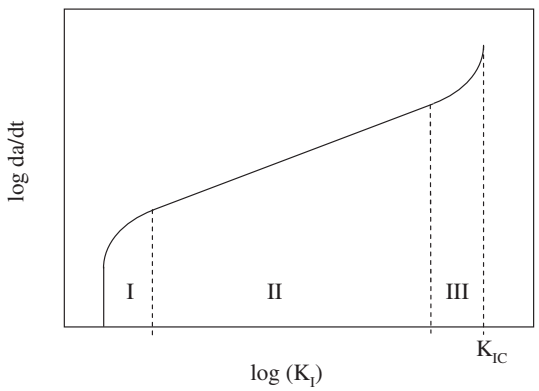

Fig. 3. Typical slow crack growth curve.

$$\log\sigma_f = \frac{1}{1+N_{scg}}\log\dot{\sigma} + \log D_{scg} \tag{10}$$

where N_{scg} and D_{scg} are referred to as the 'slow crack growth parameters' [11].

Three sources of relevant data were found in the literature for different forms of YSZ. The first data set is for 3TZP (3% mol partially stabilised zirconia) from Nemeth et al. [19], obtained through cyclic fatigue testing with reversal ratios, r, between 0.8 and −1.0. The second data set by Lowrie et al. [14] was for 8YSZ under dynamic (constant stress rate) test conditions, and the third was for 10YSZ by Choi et al. [6] again under dynamic test conditions. In Lowrie et al. [14] it is not clear whether the SCG is tested in bending or tension or what the gauge volume is, therefore assumptions have had to be made to allow the calculation of N_{scg} as follows: it has been assumed from the geometry of the test specimens that the testing is pure tension and that the gauge volume is the volume of the specimen. This approach gives a value of N_{scg} that correlates with their work.

CARES calculates the time dependent probability of failure at some time t_f, by transforming the mode 1 stress intensity at that time to t_0. For the case where the stress field is multi-axial an equivalent mode 1 stress $\sigma_{1,eq}$ with an associated $K_{1,eq}$ is calculated with a user selected multi-axial stress criteria, for example the PIA. In CARES Ψ represents the location within the body i.e. $\sigma_{1,eq,0}(\Psi)$ is the mode 1 stress at each discrete location Ψ, in the structure (in this case the finite element Gauss points) transformed from its actual value at time t to an equivalent value at time 0. The transformation of the equivalent stress distribution at time t_f to its effective stress distribution at $t = 0$ is presented in Equation (11).

$$\sigma_{1,eq,0}(\Psi) = \left[\frac{\int_0^{t_f}\sigma_{1,eq}(\Psi,t)dt}{B} + \sigma_{1,eq}^{N_{scg}-2}\left(\Psi,t_f\right)\right]^{\frac{1}{N_{scg}-2}} \tag{11}$$

where

$$B = \frac{2}{AY^2K_{1c}^{N_{scg}-2}(N_{scg}-2)} \tag{12}$$

The parameter B is an environmental/material fatigue parameter specific to CARES and for a time dependent reliability analysis using CARES it must be derived in addition to the SCG exponent N_{scg} and time independent Weibull parameters m and σ_0.

Where they are not given directly, the time-dependent properties are calculated for all of these materials to give an indication of the spread of properties that could be expected for a parametric analysis. Of the three sources of material data identified, Choi et al. [6] represents the best match for the material composition and loading regime in later analyses. The material properties from these three sources are summarised in Table 2.

The time dependent Weibull properties of Ni/8YSZ are taken to be the same as the 8YSZ ceramic matrix. Time dependent Weibull properties for LSM are not available in the literature so to allow the analysis to proceed the properties are assumed to be the same as

Table 2
Time dependent Weibull parameters of zirconia.

Material	N_{scg}	D_{scg}	B(MPa^2s)
3TZP	20 [19]	–	6×10^5 [19]
8YSZ	11 [14]	138.0	6.98×10^6
10YSZ	8 [6]	133.5 [6]	2.55×10^5

8YSZ. This will enable general trends to be investigated and discussed rather than a quantitative assessment of the cathode time-dependent probability of failure.

3. Analytical calculation – time independent failure probability

Using Equation (3) and the material properties in Table 1 the time independent probability of failure of each layer of the ceramic membrane at room temperature was calculated analytically for a range of uniform, uniaxial stresses. This simple calculation shows the difference in probability of failure of each layer at the same stress level. A plot of the probability of failure of each layer against stress in Fig. 4 shows that the cathode is most susceptible to failure under tensile stress primarily due to the low characteristic strength.

The low Weibull modulus of the cathode contributes to its high probability of failure at low stress relative to the electrolyte and anode. The effect of varying the Weibull modulus of the cathode is seen clearly in Fig. 5. As the Weibull modulus increases the slope of the curve between low probability of failure and high probability of failure increases. At very high Weibull modulus the probability of failure curve tends to a step function. This behaviour is typical of metals and the stress at which the probability of failure changes from 0 to 1 is called the ultimate tensile strength of a metal.

The 'volume effect' described previously can be observed by calculating the probability of failure of one layer (the cathode in this case) for different layer thicknesses. For a given uniform, uniaxial stress of 50 MPa as the volume increases the probability of a flaw of critical size being present also increases, the consequence of this is that the probability of failure also increases as shown in Fig. 6.

Now the probability of failure of the layers of an SOFC is calculated analytically from an analytical model of stress in a thin, multilayer plate in which the different layers have different coefficients of thermal expansion [8]. For the stress analysis the other necessary assumptions are:

- The membrane is constrained to remain flat
- The stresses are uniform through the layer thickness
- The temperature throughout the membrane is uniform and equal to 800 °C

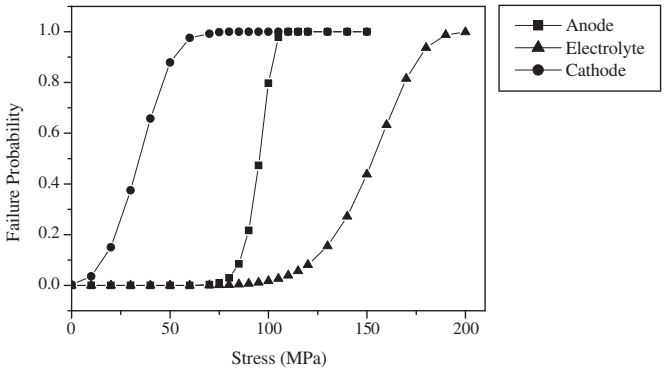

Fig. 4. Probability of failure distribution for layers in an SOFC.

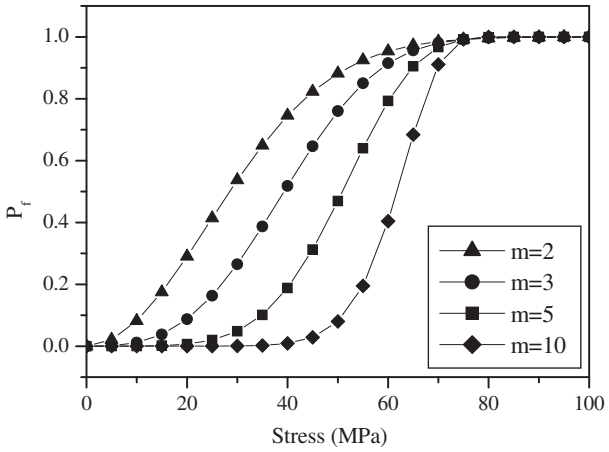

Fig. 5. Dependence of cathode probability of failure on Weibull modulus.

- In it's initial condition the membrane is stress free at 25 °C (i.e. residual stress is not included)
- The membrane is infinite in the in-plane dimensions

The equi-biaxial in-plane stresses in the layers are then calculated to be −5.26 MPa, 341 MPa and 29.1 MPa in the anode, electrolyte and cathode respectively. The probabilities of failure of the layers are given in Table 3. When residual stress is included by assuming a zero stress temperature of 1010 °C the stress distribution calculated analytically changes markedly. The in-plane stresses and corresponding probabilities of failure are shown in Table 4. The inclusion of a residual stress effectively means the temperature differential that generates layer stresses is reduced to the difference between the sintering temperature and the operating temperature, meaning the stresses are actually very low, with a correspondingly low probability of failure.

3.1. Validation of CARES method with analytical model

The CARES method was initially validated by manually calculating the probability of failure of a single element from an SOFC finite element stress analysis and comparing it to the probability of failure calculated by CARES for that element. The element chosen has cathode material properties (Table 1) and is second order type C3D20. The location and precise conditions of the stress analysis are

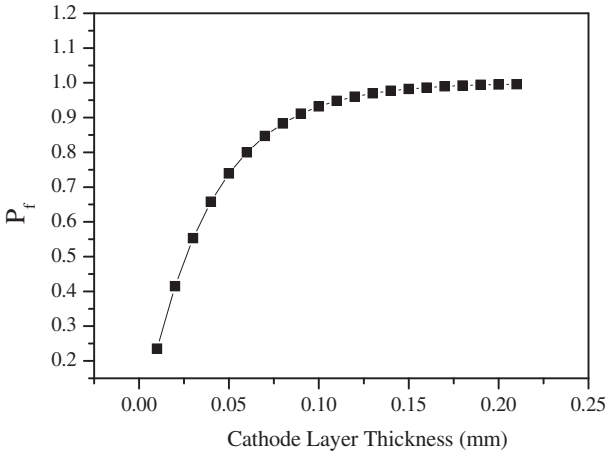

Fig. 6. Probability of failure with varying cathode thickness for $\sigma = 50$ MPa.

Table 3
Analytical calculation of P_f in ceramic membrane layers, residual stress neglected.

Layer	Stress (MPa)	P_f
Anode	−5.26	0
Electrolyte	341	1
Cathode	29.1	0.143

Table 4
Analytical calculation of P_f in ceramic membrane layers, residual stress included.

Layer	Stress (MPa)	P_f
Anode	1.46	~0
Electrolyte	−93.5	0
Cathode	−8.2	0

not important at this point as long as the elemental stresses are known and are the same for the analytical and CARES approaches. When second order finite elements are used as the input to the CARES analysis, CARES subdivides each finite element into sub-volumes centred on the element Gauss points, and uses the stresses at the Gauss points and the sub-volume for the probability of failure calculation. This helps to capture the effects of stress gradients within elements and improves the accuracy of the probability of failure calculation for the whole element. A single element (volume 2.45×10^{-12}) was used to validate CARES because the principal stresses and sub-volume (3.07×10^{-13}) at the elemental Gauss points could easily be determined and used in the analytical model by interrogating the finite element analysis results file. Stress multi-axiality was included by using the Principle of Independent Action as it is a user option in CARES. The results are presented in Table 5.

Taking the product of the probabilities of failure of the sub-volumes associated with the element Gauss points using Equation (2) gives the same probability of failure for the whole element as the output from CARES for the same element. The comparison is shown in Table 6

The effect of subdividing the element by using the Gauss points as centroids of sub-volumes can be assessed by calculating the probability of failure for the whole finite element by using the element centroidal principal stresses. This results in $P_f = 6.8 \times 10^{-7}$, a factor of two smaller than the results obtained previously. This highlights the importance of using a sufficient number of elements along stress gradients when basing the calculation of probability of failure of a structure on a finite element analysis. In this work the 'mesh independence' of the stress analysis results was confirmed by running the same elastic stress analysis a number of times with a progressively increasing number of elements. When the analysis results did not change with increasing element density the solution was considered to be independent of the element density. The stress analysis results were then cross checked with an analytical

Table 5
Probability of failure of finite element sub-volumes by analytical model.

Gauss point	σ_{11} (MPa)	σ_{22} (MPa)	σ_{33} (MPa)	P_f
1	16.5	10.6	−0.6	1.61×10^{-8}
2	28.2	15.0	−1.3	1.09×10^{-7}
3	15.6	8.8	−1.64	1.24×10^{-8}
4	30.4	15.1	−0.8	1.40×10^{-7}
5	28.3	14.6	−1.3	1.08×10^{-7}
6	32.7	29.9	−2.3	2.95×10^{-7}
7	30.2	14.6	−0.9	1.36×10^{-7}
8	35.9	33.2	−0.6	4.26×10^{-7}

Table 6
Probability of failure of single finite element by analytical model and CARES.

El. vol. (m^3)	P_f analytical	P_f CARES
2.45×10^{-12}	1.24×10^{-6}	1.24×10^{-6}

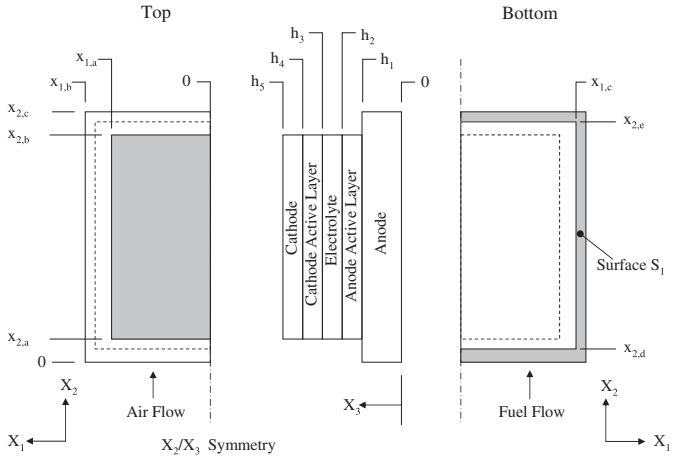

Fig. 7. SOFC geometry.

calculation of stresses in multi-layer thin plates where the individual layers have different material properties [9].

4. Time independent probability of failure of an anode supported SOFC

In the following sections a time independent and time dependent probability of failure analysis is undertaken for a typical anode supported SOFC. A finite element analysis [8] was used to calculate the stress distribution in an anode supported SOFC described in Fig. 7 and Table 7 under a variety of temperature distributions. The results of the stress analysis are used as the input to a CARES probability of failure analysis.

The probability of failure of the different layers (anode, electrolyte, cathode) was initially calculated for three different mechanical boundary condition sets BC1, BC2 and BC3 representing respectively; constraining the membrane to remain planar; allowing the membrane to bend freely; and fixing the membrane in a test housing after it has cooled from manufacture. To examine the effect of the boundary conditions only, a simple stress analysis was performed: the SOFC is initially in a zero stress state at room temperature then it's temperature is subsequently raised to 800 °C. The SOFC layers have different thermal expansion coefficients and therefore stress in induced. Stress multi-axiality was accounted for with the Principle of Independent Action. The probability of failure calculated using the analytical approach with boundary condition set BC1 is also presented for reference.

The results in Table 8 shows that when using the analytical approach the calculated probability of failure of the cathode layer is higher than the equivalent FEA/CARES method by a factor of 4. The difference is likely to be due to the computational domain being

Table 7
Dimensions of Indec ASC1 cell.

$x_{1,a} = 50$ mm	$x_{2,a} = 10$ mm	$h_1 = 600$ μm
$x_{1,b} = 60$ mm	$x_{2,b} = 110$ mm	$h_2 = 610$ μm
$x_{1,c} = 55$ mm	$x_{2,c} = 120$ mm	$h_3 = 616$ μm
	$x_{2,d} = 5$ mm	$h_4 = 626$ μm
	$x_{2,e} = 115$ mm	$h_5 = 656$ μm

Table 8
Probability of failure in layers for three different boundary conditions; BC1 – cell constrained to remain flat; BC2 – cell free to bend; BC3 – cell modelled as bonded into housing. Zero stress temperature 25 °C.

Layer	Analytical BC1	FEA BC1	FEA BC2	FEA BC3
Anode	0	0	0	0
E'lyte	1.0	1.0	1.0	1.0
Cathode	2.86×10^{-1}	6.9×10^{-2}	1.86×10^{-2}	6.37×10^{-2}

Table 9
Probability of failure in ceramic membrane layers for three different boundary conditions, zero stress temperature 1010 °C.

Layer	FEA – BC1	FEA – BC2	FEA – BC3
Anode	0	0	0
E'lyte	0	0	0
Cathode	0.5×10^{-10}	0.5×10^{-10}	2.18×10^{-6}

finite in the finite element model but infinite in the analytical model. If the analytical model was used to analyse the design it could lead to a substantial over-design of the structure.

The probability of failure calculation is now repeated with residual stress included i.e. the zero stress temperature is taken as 1010 °C, chosen to represent the point at which the SOFC supports elastic strain on cooling from sintering [3]. The results, presented in Table 9 shows that the inclusion of residual stress significantly changes the calculated stresses and therefore the probability of failure in each layer.

4.1. Uniform and detailed temperature distribution

To make the probability of failure calculation more representative of a real SOFC a CFD model was used to calculate the temperature distribution at discrete SOFC operating current densities of 70 mA cm^{-2}, 200 mA cm^{-2} and 300 mA cm^{-2} and the resulting temperature distribution used as nodal temperatures in a finite element stress analysis [8]. An example of the temperature distribution, at 300 mA cm^{-2}, is shown in Fig. 8.

The results of the stress analysis were then used as input to a CARES probability of failure analysis as in the previous analysis. The results of this analysis are shown in Table 10. From these results it is evident that the use of representative temperature distribution is important. Although the mean temperature for the T_{300mA} case is close to 800 °C, the probability of failure is more than a factor of 3 different to the uniform temperature $T_{800°C}$ case due to the stresses induced by in-plane temperature gradients.

Failure probabilities of the order of 10^{-11} or 10^{-13} are too small to be meaningful and would be practically taken to be equal to zero, they are presented here for completeness only.

4.2. Evolution of time independent probability of failure

When the stress state is time-varying it makes physical sense to refer to the cumulative distribution function (CDF), introduced in Section 2 as the 'actual' probability of a component having failed by a given time. The stress distribution in an SOFC will change over time as its temperature changes due to, for example changes in electrical load conditions. A simplified duty cycle was developed previously [8] for an SOFC and is shown in Fig. 9. The zero stress state is at 1010 °C at time $t = 0$.

At time $t_1(>0)$ the CDF for an individual finite element (or sub-element) is calculated by taking the peak elemental stress in the time period $t = 0$ to $t = t_1$. The component failure probability is then given by the product of these maximum elemental failure probabilities according to Equation (2).

Fig. 10 shows P_f and CDF in the cathode layer for a time varying stress state induced by the duty cycle. When the first operating current of 70 mA cm^{-2} is applied at 20 h the failure probability increases notably because of in-plane temperature gradients. At 2020 h the power level changes to 300 mA m^{-2} inducing larger in-plane temperature gradients and leading to a further increased failure probability. When the power level is reduced at 4020 h to 160 mA m^{-2}, P_f decreases while the CDF remains constant. Finally the in-plane temperature gradients are removed and the fuel cell is cooled to room temperature, the net result being a decrease in P_f, while the CDF stays at its maximum value.

Fig. 11 shows the evolution of the CDF in the anode, electrolyte and cathode over the duty cycle. The failure probability in the electrolyte is diminishingly small as the stress field is

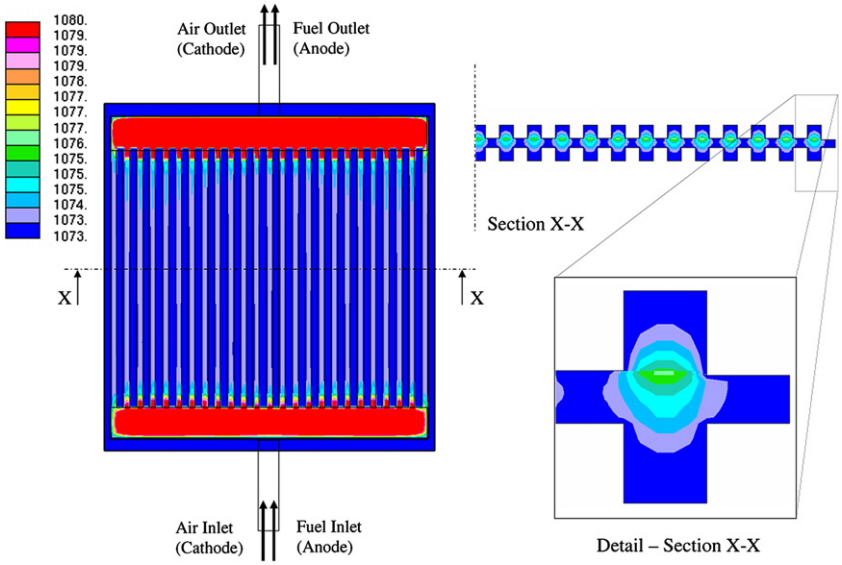

Fig. 8. Temperature distribution at 300 mA cm^{-2}.

Table 10
Probability of failure in ceramic membrane layers for uniform and CFD temperature boundary conditions, BC3, zero stress at 1010 °C.

Temp BCs	T_{800}	T_{cfd1}	T_{cfd2}	T_{cfd3}
Anode	0	2.81×10^{-11}	2.82×10^{-11}	2.85×10^{-11}
E'lyte	0	2.4×10^{-13}	2.4×10^{-13}	2.4×10^{-13}
Cathode	2.18×10^{-6}	9.25×10^{-6}	2.09×10^{-5}	4.26×10^{-5}

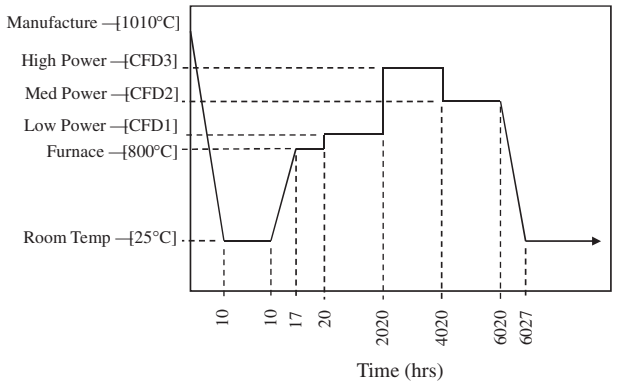

Fig. 9. Simplified SOFC duty cycle.

predominantly compressive. In this analysis the CDF is highest in the cathode layer and lowest in the electrolyte.

5. Time dependent failure of a SOFC ceramic membrane

The time dependent probability of failure was defined at the beginning of this paper as the increasing probability of failure of a component over time due to SCG. In order to isolate and quantify the effects of SCG, the probability of failure was calculated for the anode supporting layer when the SOFC is subject to uniform, constant temperature of 800 °C with mechanical boundary condition set BC3 applied. P_f is shown to increase with increasing time in Fig. 12 for constant B (Equation (11)) and varying N_{scg}. In Fig. 13 the effect of varying B while holding N_{scg} constant can be seen.

The time dependent material data available in the literature is inconsistent and sparse. To assess the impact of this variation in material properties data from Choi et al. [7] and Nemeth et al. [19] (see Table 2) were used to calculate the time dependent probability

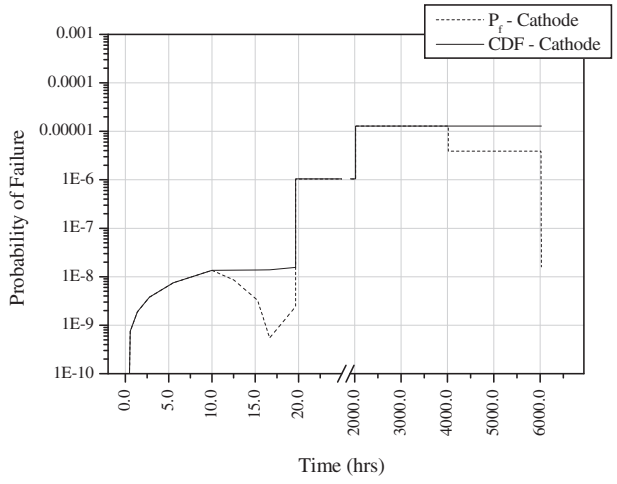

Fig. 10. P_f and CDF of cathode layer over SOFC duty cycle.

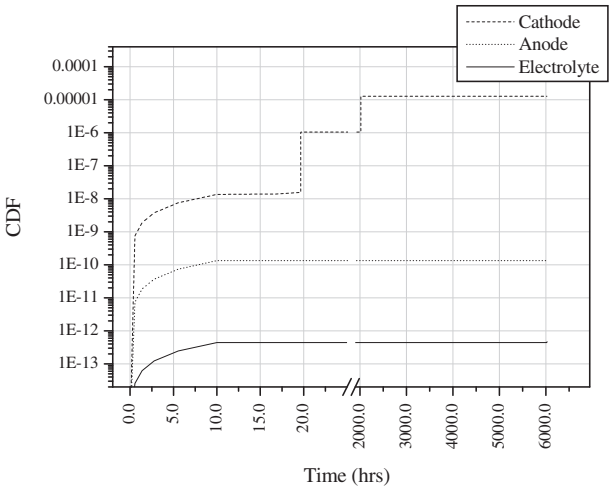

Fig. 11. CDF of anode, cathode and electrolyte layers over SOFC duty cycle.

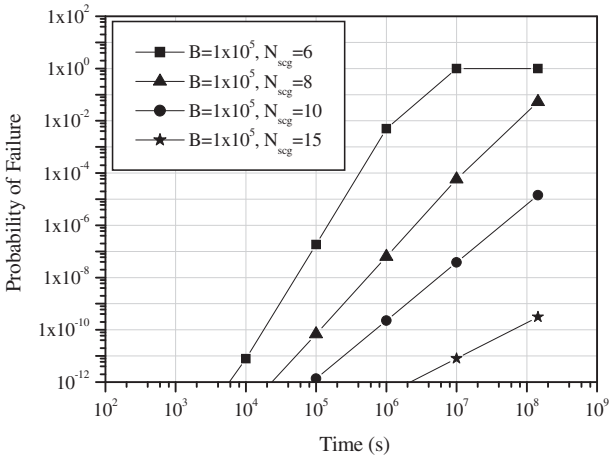

Fig. 12. Dependence of cathodic time dependent P_f on N_{scg} in SOFC at uniform constant temperature 800 °C.

of failure for an 800 °C uniform temperature case with a zero stress temperature of 1010 °C, the results are shown in Fig. 14. The probability of failure increases over time as SCG degrades the ability of the material to sustain the applied load. It is interesting to note that at time $t = 0$, $P_{f,an}$ is less than 1×10^{-14} and considerably below

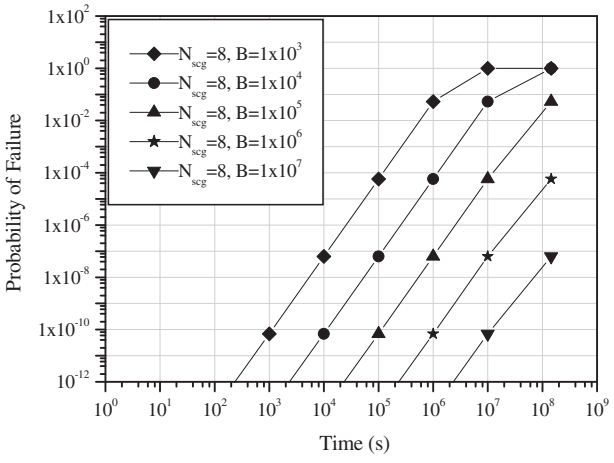

Fig. 13. Dependence of cathodic time dependent P_f on B in SOFC at uniform constant temperature 800 °C.

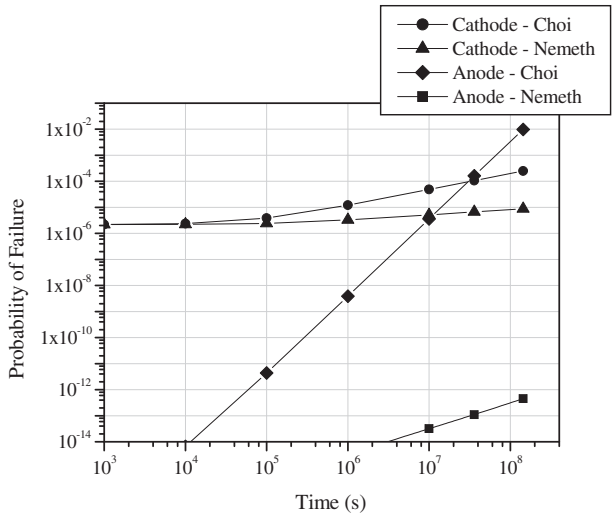

Fig. 14. Time dependent P_f for anode and cathode under uniform constant temperature loading of 800 °C.

that of the cathode at 2.18×10^{-6}. With the material properties derived from Nemeth et al. [19] the probability of failure of the anode remains below that of the cathode up to $t = 1.44 \times 10^8$ s. However, with the material properties derived from Choi et al. [7], at approximately time $t = 4 \times 10^7$ s, the relationship becomes inverted and $P_{f,an}$ subsequently increases more quickly with time than $P_{f,ca}$.

5.1. Time dependent failure probability over duty cycle

Fig. 15 shows the evolution of the CDF calculated from the time dependent probability of failure over the duty cycle. The effect of SCG is particularly apparent when Figs. 11 and 15 are compared. The final probability of failure of the cathode layer is 1.28×10^{-5} for the time independent analysis compared to 1.24×10^{-3} for the time dependent probability of failure analysis, showing that SCG increases the probability of failure of the cathode layer by two orders of magnitude over the duty cycle. For the anode the change is larger still with the probability of failure at the end of the duty cycle being almost insignificant when SCG is not included (Fig. 11) to 0.54 when it is (Fig. 15). Fig. 15 shows that in the time periods 20–2020 h, 2020–4020 h, and 4020–6020 h the effect of SCG is to increase the failure probability over time even though the temperature distribution in the fuel cell is unchanging.

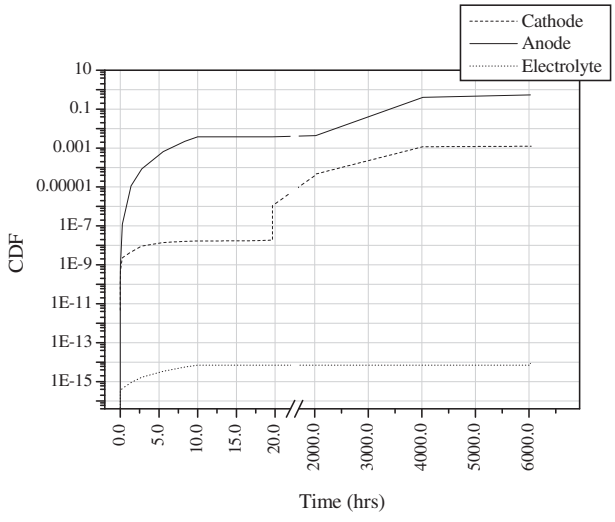

Fig. 15. Probability of failure of membrane layers over detailed temperature duty cycle assuming visco-plasticity and SCG, using material properties from Choi et al. [6].

6. Concluding remarks

In this paper the time-independent and time-dependent failure probability of the layer volumes in an SOFC have been calculated under a range of idealised conditions using an analytic model and the software package CARES. The calculated probability of failure applies to the cracking of layer volumes only, no account has been taken of the delamination of SOFC layers, which is another observed failure mode of SOFCs. Taking account of the 'probability of delamination' would be a useful next step for this analysis.

The time-independent failure probability was also used to assess the impact of using detailed temperature distribution from a CFD model instead of assuming a uniform furnace temperature throughout the ceramic membrane. The largest difference in predicted failure probability occurred when the temperature gradients predicted by the CFD model were largest i.e. at the highest operating current. In this case the failure probability for the 300 mA cm^{-2} condition is a factor of 20 higher than the uniform temperature condition, T_{800}. While not as significant as the effect of changing the mechanical boundary conditions this is nevertheless an important consideration.

The models indicate that over a duty cycle the time-independent failure probability of each of the layer volumes increases and decreases in step with the layer stresses. To make physical sense the failure probability of the membrane cannot decrease as time goes on so the concept of a cumulative distribution function was introduced that will never decrease with increasing time. In this way the stress history of a component is accounted for in the probability of failure calculation, but this is not to say that the CDF is time-dependent, it merely represents the highest probability of failure that the component has experienced to that point in its history.

The time-dependent probability of failure accounting for subcritical crack growth has been calculated for the uniform temperature and detailed duty cycles. The results of the analysis indicate that the bulk strength of ceramics used in SOFCs decreases significantly through slow crack growth, leading to increased probability of failure over their operational lifetime. The range of material properties available in the literature has been shown to produce large differences in the predicted time dependent failure probability. In order to quantitatively predict the lifetime of SOFC ceramic components specific material testing would have to be done to ensure that the material properties were appropriate. It has been shown that for a given stress level SCG acts to significantly increase the probability of failure over time.

References

[1] M.F. Ashby, D.R.H. Jones, Engineering Materials 1: An Introduction to Their Properties and Applications, Pergamon Press, 1980.
[2] A. Atkinson, T.M.G.M. Ramos, Solid State Ionics, Diffusion and Reactions 129 (1–4) (2000) 259–269.
[3] A. Atkinson, A. Selcuk, Acta Materialia 47 (3) (1999) 867–874.
[4] A. Atkinson, A. Selcuk, Solid State Ionics, Diffusion and Reactions 134 (1–2) (2000) 59–66.
[5] S.B. Batdorf, J.G. Crose, Journal of Applied Mechanics 41 (2) (1974) 459–464.
[6] S.R. Choi, N.P. Bansal, Journal of the American Ceramic Society 88 (6) (2005) 1474–1480.
[7] S.R. Choi, N.N. Nemeth, J.P. Gyekenyesi, Fatigue and Fracture of Engineering Material and Structures 28 (5) (2005) 489–497.
[8] R. Clague. The Probability of Failure of Solid Oxide Fuel Cells by the Integrated Modelling of Multiple Physical Processes, PhD thesis, Imperial College London, 2008.

[9] R. Clague, A.J. Marquis, N.P. Brandon, Finite element and analytical stress analysis of a solid oxide fuel cell, Journal of Power Sources 210 (2012) 224–232.
[11] American Society for Testing and Materials, Annual Book of ASTM Standards, vol. 15.01, American Society for Testing and Materials, Volume ASTM C 1465, Test Method for Determination of Slow Crack Growth Parameters of Advanced Ceramics by Constant Stress-Rate Flexural Testing at Elevated Temperatures, West Conshohocken, Pa: ASTM, 2001.
[12] B. Gross, J.P. Gyenkenyesi, Journal of the American Ceramic Society 73 (3) (1989) 506–507.
[13] J.P. Gyekenyesi, Transactions of the ASME. Journal of Engineering for Gas Turbines and Power 108 (3) (1986) 540–546.
[14] F.L. Lowrie, R.D. Rawlings, Journal of the European Ceramic Society 20 (6) (2000) 751–760.
[15] J.R. Lund, J.P. Byrne, Civil Engineering and Environmental Systems 18 (3) (2001) 243–250.
[16] J.J. Masson, E. Bourgain, International Journal of Fracture 55 (4) (1992) 303–319.
[17] C.S. Montross, H. Yokokawa, M. Dokiya, British Ceramic Transactions 101 (3) (2002) 85–93.
[18] A. Nakajo, C. Stiller, G. Harkegard, O. Bolland, Journal of Power Sources 158 (1) (2006) 287–294.
[19] N.N. Nemeth, L.M. Powers, L.A. Janosik, J.P. Gyenkenyesi, CARES/Life Ceramics Analysis and Reliability Evaluation of Structures Life Prediction Program, User Guide, NASA Technical Publications, 2003, TM-2003–106316.
[20] S.S. Pai, J.P. Gyekenyesi, Calculation of the Weibull Strength Parameters and Batdorf Flaw Density Constants for Volume and Surface Flaw Induced Fracture in Ceramics, NASA Technical Publications, 1988, TM-100890.
[21] D.N. Prabhakar-Murthy, M. Xie, R. Jiang, Weibull Models, Wiley, 2003.
[22] M. Radovic, E. Lara-Curzio, G. Nelson, Fracture Toughness and Slow Crack Growth Behavior of Ni-YSZ and YSZ as a Function of Porosity and Temperature (2006). pp. 373–81.
[23] P. Rosin, E. Rammler, Journal of the Institute of Fuel 7 (31) (1933) 29–36.
[24] A. Selimovic, M. Kemm, T. Torisson, M. Assadi, Journal of Power Sources 145 (2) (2005) 463–469.
[25] T.T. Shih, Engineering Fracture Mechanics 13 (2) (1980) 257–271.
[26] Conneticut Reserve Technologies, CARES/Life Ceramics Analysis and Reliability Evaluation of Structures Life Prediction Program, Theory Guide (2006).
[27] W. Weibull, Statistical Theory of Strength of Materials (151), In: Ingeniors Vetenskaps Akademien – Handlingar, vol. 45 (1939).
[28] D. Yanhai, N.M. Sammes, G.A. Tompsett, Z. Deliang, J. Swan, M. Bowden, Journal of the Electrochemical Society 150 (1) (2003) 74–78.
[29] F.T. Pierce, Journal of Textile Institute 17 (1926) 355.